DOI: 10.19884/j.1672-5220.202406004

F-B Co-Doped TiO_2 Nanosheets Bounded with Highly Active Anatase (001) Facets for Improved Photocatalytic Hydrogen Evolution

ZHANG Mengyao, WEI Li, LIU Lei*
Center for Advanced Low-dimension Materials, Donghua University, Shanghai 201620, China

Abstract: F-B co-doped TiO_2 nanosheets with exposed anatase (001) facets were synthesized via a one-pot solvothermal method, and their photocatalytic hydrogen evolution performance was investigated. Characterization results confirm that this method effectively promotes the growth of the highly active anatase (001) facets and enhances visible and infrared light absorption while inducing oxygen vacancies. Under optimal conditions, the hydrogen evolution reaches 20.57 μmol after 10 h of ultraviolet-visible (UV-Vis) light irradiation, exceeding the commercial TiO_2 nanoparticles Degussa P25 by more than 10 times. These findings highlight the potential of F-B co-doped TiO_2 nanosheets for efficient photocatalysis.

Keywords: F-B co-dope; TiO_2; photocatalysis; active facet; oxygen vacancy
CLC number: O614; O643 **Document code**: A
Article ID: 1672-5220(2025)05-0457-09

Open Science Identity (OSID)

0 Introduction

In 1972, Fujishima et al.[1] first reported the successful use of the photoelectrochemical method to harness solar energy for water splitting on TiO_2 electrodes. Since then, due to its advantages including high stability, high electron transferability, non-toxicity and low cost, TiO_2 has been widely applied as a robust photocatalyst in various fields such as energy and environment[2-3]. However, its wide bandgap (anatase, 3.2 eV; rutile, 3.0 eV) limits its absorption to ultraviolet (UV) light, rendering it unable to utilize visible light in sunlight. Meanwhile, the photocatalytic activity of TiO_2 is further restricted by some other factors such as rapid recombination of photoinduced electron-hole pairs and the hydrogen-oxygen reverse reaction. Therefore, in order to improve the photocatalytic activity of TiO_2, it is crucial to enhance its visible light responsiveness, and inhibit the recombination of electron-hole pairs and the hydrogen-oxygen reverse reaction. Current methods for this purpose are mainly focused on the following pathways, including morphology control, element doping, dye sensitization and compositing with other materials[4-5].

Morphology control mainly involves restricting the growth of crystal facets with low catalytic activity while exposing those with high catalytic activity[6]. Due to the high surface energy and the exposure of atoms with a low coordination number, as well as a wide Ti—O—Ti bond angle, anatase (001) facets exhibit higher catalytic activity over other facets, which has been indicated by both theoretical calculations[7-8] and experimental results[9-10]. By using hydrofluoric acid (HF) as a crystal growth modifier, Yang et al.[11] first synthesized anatase single crystals with a 47% exposure ratio of anatase (001) facets via a hydrothermal method. Inspired by this pioneering work, researchers have continuously increased the exposure ratio of anatase (001) facets by selecting different crystal growth modifiers and optimizing reaction conditions. The exposure ratio of anatase (001) facets can reach 64% under the synergies of isopropanol and HF[12], while by controlling the amount of HF and the hydrothermal reaction temperature, the exposure ratio can further increase to 89%[13]. In a pure isopropanol system, using diethylenetriamine (DETA) as the crystal growth modifier, anatase ultrathin layers with nearly 100% exposed anatase (001) facets can be obtained[14]. Recently, the influence of precursor resource[15], reaction temperature[16-17], ripening environment[18] and synthesis strategy[19-20] on the controlled exposure of anatase (001) facets has been extensively investigated. However, almost all the samples reported in the above studies only exhibit UV-responsive characteristics, which means that they can only perform the photocatalytic tasks under UV light irradiation.

Element doping can form new energy levels in the bandgap, thereby reducing the TiO_2 bandgap energy, expanding the light response range to the visible light region, and lowering the rate of recombination of photoinduced electron-hole pairs. It is a simple and effective method to improve the photocatalytic activity of TiO_2[21-22]. Several metal elements, especially transition

Received date: 2024-06-13
Foundation item: National Natural Science Foundation of China (No. 81861138040)
* Correspondence should be addressed to LIU Lei, email: liulei@dhu.edu.cn
Citation: ZHANG M Y, WEI L, LIU L. F-B co-doped TiO_2 nanosheets bounded with highly active anatase (001) facets for improved photocatalytic hydrogen evolution[J]. *Journal of Donghua University (English Edition)*, 2025, 42(5): 457-465.

metal elements, have been used for TiO_2 doping. However, the doping of metal elements reduces the thermal stability of TiO_2 and introduces additional active centers, resulting in an elevated recombination of photoinduced electron-hole pairs[23]. Therefore, since Asahi et al.[24] first reported in 2001 that N-doped TiO_2 exhibited enhanced visible light responsiveness and photocatalytic performance, non-metal element doping has gradually become a hot research topic. Non-metal element doping is difficult to affect the TiO_2 conduction band structure. Instead, it is usually achieved by reconstructing the TiO_2 valence band, shifting it upward to narrow the bandgap. This can significantly reduce the electronegativity of TiO_2 and greatly enhance its absorption of visible light. Commonly used non-metal elements for TiO_2 doping include carbon, nitrogen, sulfur and others with approximate atomic radius as oxygen[25-26]. Sol-gel, hydrothermal and co-precipitation methods can all be applied to synthesize non-metal element-doped TiO_2[27-28]. However, these doped TiO_2 materials generally exist in the morphological form of nanoparticles or nanoparticle assemblies. Non-metal element co-doped TiO_2 photocatalysts with a specific and uniform morphology are rarely reported.

Recent studies have found that oxygen vacancies play an important role in enhancing the catalytic activity of TiO_2 in heterogeneous catalytic reactions. Nakamura et al.[29] demonstrated that plasma-treated TiO_2 containing oxygen vacancies exhibited significantly enhanced photocatalytic degradation of NO. A similar enhancement effect was also reported by Justicia et al.[30]. In addition to modifying the electronic structure, oxygen vacancies can provide important reaction sites for reactant molecules[31]. Although there are various methods to induce the formation of oxygen vacancies, such as heat treatment in vacuum, inert atmosphere or reducing atmosphere[32], these methods display many obvious drawbacks, such as complex equipment, harsh synthesis conditions and high cost. Therefore, it is still a very important challenge to promote the formation of oxygen vacancies through a simple and direct method.

In this study, F-B co-doped TiO_2 (F-B-TiO_2) nanosheets with highly active anatase (001) facets, were synthesized through a simple one-pot solvothermal method. F-B co-doping significantly enhances the absorption of visible light by the as-synthesized TiO_2 and induces the formation of oxygen vacancies in the TiO_2 matrix. Compared to non-doped TiO_2, F-B-TiO_2 nanosheets demonstrate significantly improved photocatalytic performance for hydrogen evolution from water under UV-visible (UV-Vis) light irradiation.

1 Materials and Methods

1.1 Chemical reagents

All chemical reagents are of analytical grade and used without further purification. Hydrofluoboric acid (HBF_4), titanium trichloride ($TiCl_3$) and anhydrous ethanol were purchased from Shanghai Chemical Reagent Co., Ltd., China. Commercial TiO_2 nanoparticles Degussa P25 (P25 for short) were bought from Sigma-Aldrich (Shanghai) Trading Co., Ltd., China and used as a reference material for photocatalytic hydrogen evolution.

1.2 Synthesis of F-B-TiO_2 nanosheets

F-B-TiO_2 nanosheets were synthesized by using a simple one-pot solvothermal method. In a typical synthesis, a certain amount of $TiCl_3$ solution was added dropwise into 60 mL ethanol followed by stirring for 5 min. Subsequently, different amounts of HBF_4 were added, by which the volume of $TiCl_3$ was controlled to maintain a series of volume ratios with HBF_4. After thorough mixing, the mixture was transferred into a 100 mL Teflon-lined stainless-steel autoclave and maintained for solvothermal treatment. The reaction was conducted at 200 ℃ for 12 h. After natural cooling, the samples were successively washed with deionized water and ethanol three times, respectively, and dried overnight at 60 ℃ in an oven. For simplicity, F-B-TiO_2-X is used to denote different samples synthesized at various volume ratios of HBF_4 to $TiCl_3$, where X represents the volume ratio of HBF_4 to $TiCl_3$ ($v(HBF_4):v(TiCl_3)$). If $X=0$, it means there is no HBF_4 added during sample preparation.

1.3 Characterization

The obtained F-B-TiO_2 nanosheets were characterized by X-ray diffraction (XRD), UV-Vis-near Infrared (UV-Vis-NIR) absorption spectroscopy, X-ray photoelectron spectroscopy (XPS), scanning electron microscopy (SEM) and transmission electron microscopy (TEM). XRD data were obtained by using a Philips X' Pert PRO SUPER X-ray diffractometer (PANalytical, the Netherlands) (Cu Kα, $\lambda = 1.540\,56 \times 10^{-10}$ m) with an operating voltage and current of 40 kV and 40 mA, respectively. XPS spectra were acquired by using an ESCALAB 250Xi X-ray photoelectron spectrometer (Thermo Fisher Scientific, USA). UV-Vis-NIR absorption spectra were measured on a UV-2600 UV-Vis spectrophotometer (Shimadzu, Japan). SEM images were obtained with a SUPRATM 40 field emission scanning electron microscope (Carl Zeiss, Germany) and TEM images were obtained with a JSM-2010F transmission electron microscope (JEOL Ltd., Japan).

1.4 Photocatalytic activity testing

The photocatalytic activity of F-B-TiO_2 samples was evaluated through photocatalytic hydrogen evolution experiments. The experiments were conducted in a closed system (500 mL) connected to a gas chromatography, with a 150 W xenon lamp as the light source (irradiation from the top). F-B-TiO_2 (0.1 g) was dispersed in a 100 mL mixture of water and methanol (a volume ratio of 9∶1). The amount of hydrogen evolution was directly detected online by gas chromatography.

2 Results and Discussion

2.1 Crystal structure analyses

Figure 1 shows the XRD patterns of some as-prepared F-B-TiO_2 samples in this experiment. Three samples were selected for XRD test: F-B-TiO_2-0 (a), F-B-TiO_2-0.50 (b) and F-B-TiO_2-0.75 (c). It can be seen that all the samples synthesized under different conditions exhibit pure anatase phase (JCPDS card No. 21-1272), since all the identified peaks can be perfectly indexed to representative anatase crystal facets. The sharp and strong diffraction peaks indicate good crystallinity of the F-B-TiO_2 samples.

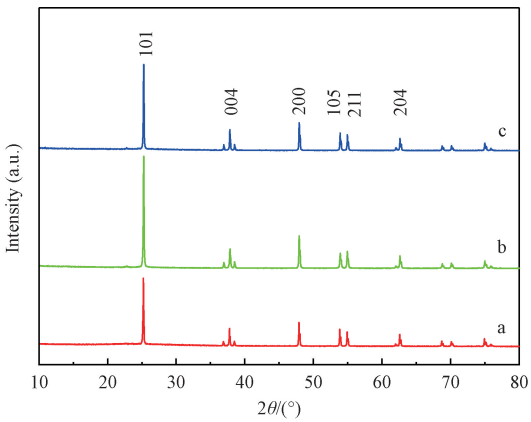

Fig. 1 XRD patterns of F-B-TiO_2 samples obtained at different volume ratios of HBF_4 to $TiCl_3$

2.2 Morphology characterization

The microscopic morphology, particle size and exposed crystal facets of F-B-TiO_2 samples were characterized by SEM and TEM. In the absence of HBF_4, the apparent color of the obtained sample is pure white as illustrated in the inset of Fig. 2(a). Its typical microscopic morphology is spherical aggregates composed with irregular building blocks, of which the exposed crystal facets are almost all anatase (101) facets with low activity (red arrows in Fig. 2(a)). When a small amount of HBF_4 was added (where the volume ratio of HBF_4 to $TiCl_3$ is 0.25), the apparent color of the final sample becomes slight grey. The microscopic structure changes from spherical to a flower-like structure composed of nanoplates with a thickness of about 150 nm (Fig. 2(b)). The exposure percentage of anatase (101) facets decreases significantly (red arrows in Fig. 2(b)), while some exposed anatase (001) facets can be identified (blue arrows in Fig. 2(b))[11]. With an increased addition of HBF_4 to a volume ratio of HBF_4 to $TiCl_3$ of 0.50, the apparent color of the sample changes into blue-gray as shown in the inset of Fig. 2(c). The obtained flower-like structures separate from each other (Fig. 2(c)) instead of agglomerating together like the samples synthesized at a lower HBF_4 to $TiCl_3$ volume ratio (Fig. 2(b)). From the magnified SEM image, it can be found that the building blocks exhibit a more pronounced sheet-like structure (Fig. 2(d)). Although the diameters of the nanosheets vary slightly from each other, their thicknesses are quite uniform at around 70 nm. Compare with previous reports[11-12], the edges of the nanosheets comprising the building blocks exhibit a relatively smooth and round surface, instead of displaying clear intersection lines of (101) and (001) facets or two (101) facets. Additionally, the exposed anatase (001) facets are not very smooth and intact but exhibit many recesses and pore structures as shown in Fig. 2(d). This phenomenon is further verified by the TEM image (Fig. 2(e)), in which the defects can be easily recognized by lower contrast in the sample sheet. Since the lengths of F-B-TiO_2 nanosheets are located between 0.5 and 1.5 μm, the exposure percentage of anatase (001) facets is estimated to be between 75% and 90%, which can be calculated by using ideal anatase single crystal as a model system. Further increasing HBF_4 to a volume ratio of HBF_4 to $TiCl_3$ of 0.75, it can be observed that the total amount of nanosheet-like structures decreases, and many nanometer-sized particles appear on the flower-like aggregates (Fig. 2(f)).

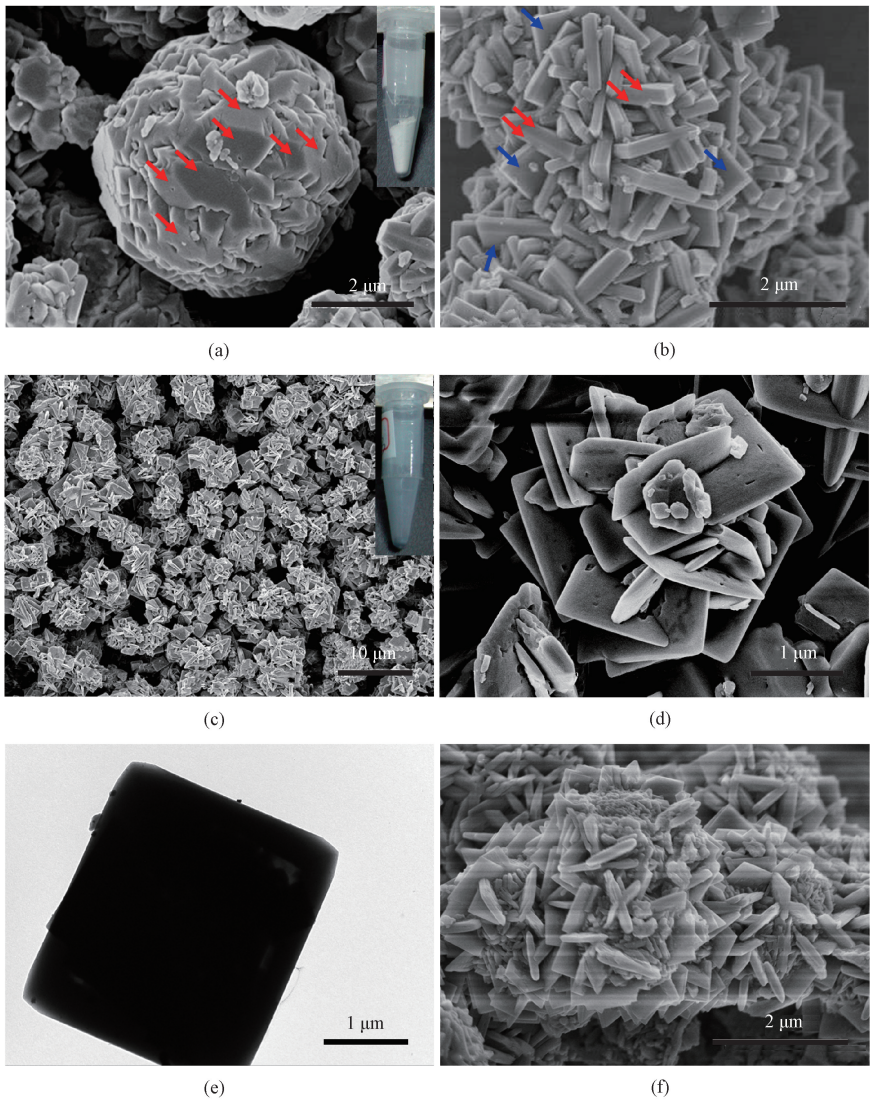

Fig. 2 SEM and TEM images of F-B-TiO_2 samples obtained at different volume ratios of HBF_4 to $TiCl_3$: (a) SEM image of F-B-TiO_2-0; (b) SEM image of F-B-TiO_2-0.25; (c)–(d) SEM images of F-B-TiO_2-0.50; (e) TEM image of F-B-TiO_2-0.50; (f) SEM image of F-B-TiO_2-0.75

2.3 Photo-responsive properties

The UV-Vis-NIR spectroscopy was utilized to analyze the photo-responsive properties of F-B-TiO_2 samples synthesized at different volume ratios of HBF_4 to $TiCl_3$. P25 was chosen as a reference material here. The UV-Vis-NIR results shown in Fig. 3(a) indicate that both P25 and all F-B-TiO_2 samples have nearly overlapping absorption spectra below 400 nm, which mainly reflects the intrinsic absorption of anatase TiO_2 materials[33]. The sample synthesized without adding HBF_4 exhibits a similar absorption spectrum to P25, with absorption mainly concentrated in the UV region and no absorption in the visible and infrared regions. When HBF_4 is added into the synthesis system, the absorption spectra undergo significant changes, exhibiting strong absorption above 400 nm up to the infrared region. This absorption is mainly caused by the excitation of electrons localized in the defect structure states which are below the conduction band edge of anatase TiO_2, induced by low-energy photon or thermal excitation[34]. It can also be easily observed that the absorbance of F-B-TiO_2 samples reaches the maximum when the volume ratio of HBF_4 to $TiCl_3$ is 0.50.

According to previous studies[35-36], bandgap energies of the obtained samples were determined by

$$\alpha h\nu = A(h\nu - E_g)^p, \quad (1)$$

where α, $h\nu$, A and E_g represent the adsorption coefficient, photon energy, proportionality constant and bandgap energy, respectively; p is the bandgap scaling exponent, with $p = 1/2$ for the direct bandgap and $p = 2$ for the indirect bandgap. Since anatase is an indirect bandgap semiconductor, the bandgap energy can be

estimated by extrapolating the linear portion of $(\alpha h\nu)^{1/2}$ versus $h\nu$ plot in Fig. 3(b). It is found that the co-doping of F and B can reduce the bandgap energy of the samples compared to P25. The lowest bandgap energy with a value of 2.87 eV is achieved for F-B-TiO_2-0.50, which is consistent with UV-Vis-NIR results.

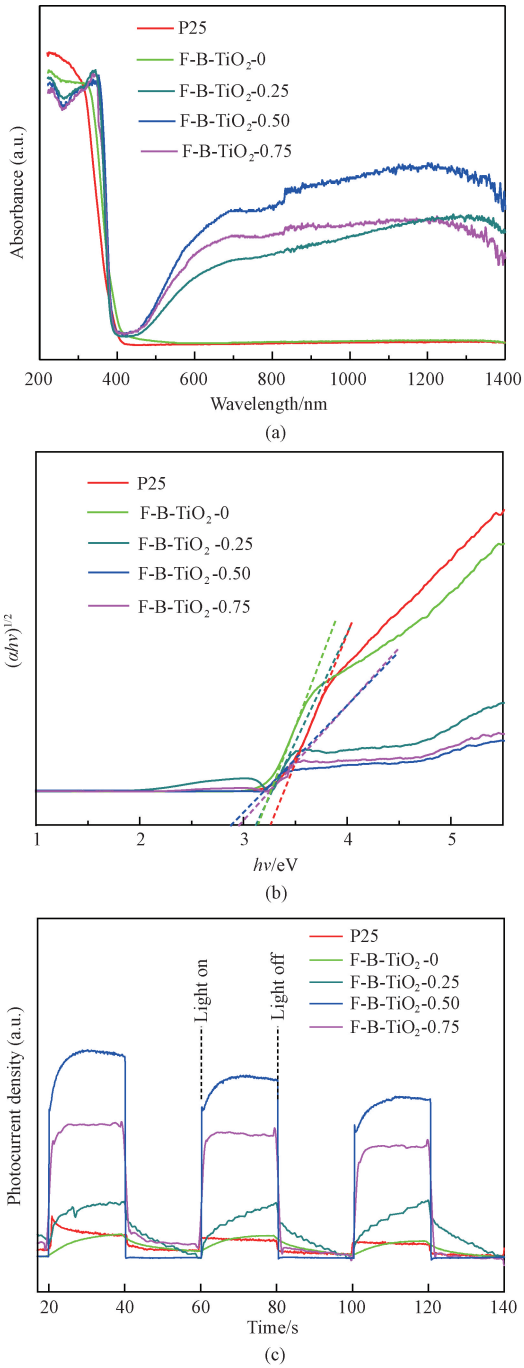

Fig. 3 Photo-responsive properties of P25 and four F-B-TiO_2 samples obtained at different volume ratios of HBF_4 to $TiCl_3$: (a) UV-Vis-NIR spectra; (b) corresponding bandgap energies; (c) transient photocurrent response

2.4 Photoelectrochemical and surface chemical analyses

Transient photocurrent measurements under chopped light irradiation were conducted on P25 and four F-B-TiO_2 samples by using a xenon lamp as the light source. The results shown in Fig. 3(c) indicate that the photocurrent rapidly rises and falls with the light being switched on and off, indicating a higher charge separation rate under light irradiation. The F-B-TiO_2-0.50 sample displays the maximum photocurrent response for all the tested samples. This significant enhancement illustrates higher separation efficiency of the photogenerated electron-hole pairs, which benefits from the lower reaction barrier and higher photocatalytic activity.

The composition and element state of the F-B-TiO_2-0.50 sample were characterized by using the XPS analysis. The elements presented in the sample mainly include Ti, O, F, B and C as shown in the survey scan in Fig. 4(a). The binding energy of O 1s is located at 528.4 eV (Fig. 4(b)). It is in good agreement with the typical value of lattice oxygen in anatase reported in previous studies[37-38]. The XPS spectrum of Ti 2p displays two peaks at binding energies of 462.9 and 457.1 eV (Fig. 4(c)), which could be assigned to Ti $2p_{1/2}$ and Ti $2p_{3/2}$, respectively. It is worth noting that these values are slightly lower than those of unmodified TiO_2 (465.0 eV for Ti $2p_{1/2}$ and 459.5 eV for Ti $2p_{3/2}$). This result is probably led by the increase in the electron density with the expected decrease in the oxidation state of Ti atoms, which implies the existence of Ti^{3+} ions. Considering the experimental process, the appearance of Ti^{3+} ions is mainly due to the substitution of F and the generation of oxygen vacancies. Similar process has been reported in a fluorinated TiO_2 system by Czoska et al.[39]. The XPS spectrum of F 1s has a peak centered at around 682.9 eV (Fig. 4(d)), which is originated from the F species in the form of $TiOF_2$ and/or $\equiv$Ti—F on the crystal surface of anatase[11, 40]. There is only one weak peak centered at 192.4 eV in B 1s spectrum (Fig. 4(e)). Two possible reasons have been proposed to explain such a phenomenon in B modified TiO_2 systems, including a low concentration of doped B[25] and poor XPS measurement sensitivity for B[41]. The presence of C is also confirmed by XPS (Fig. 4(f)), which is possibly led by the contamination during the synthesis process.

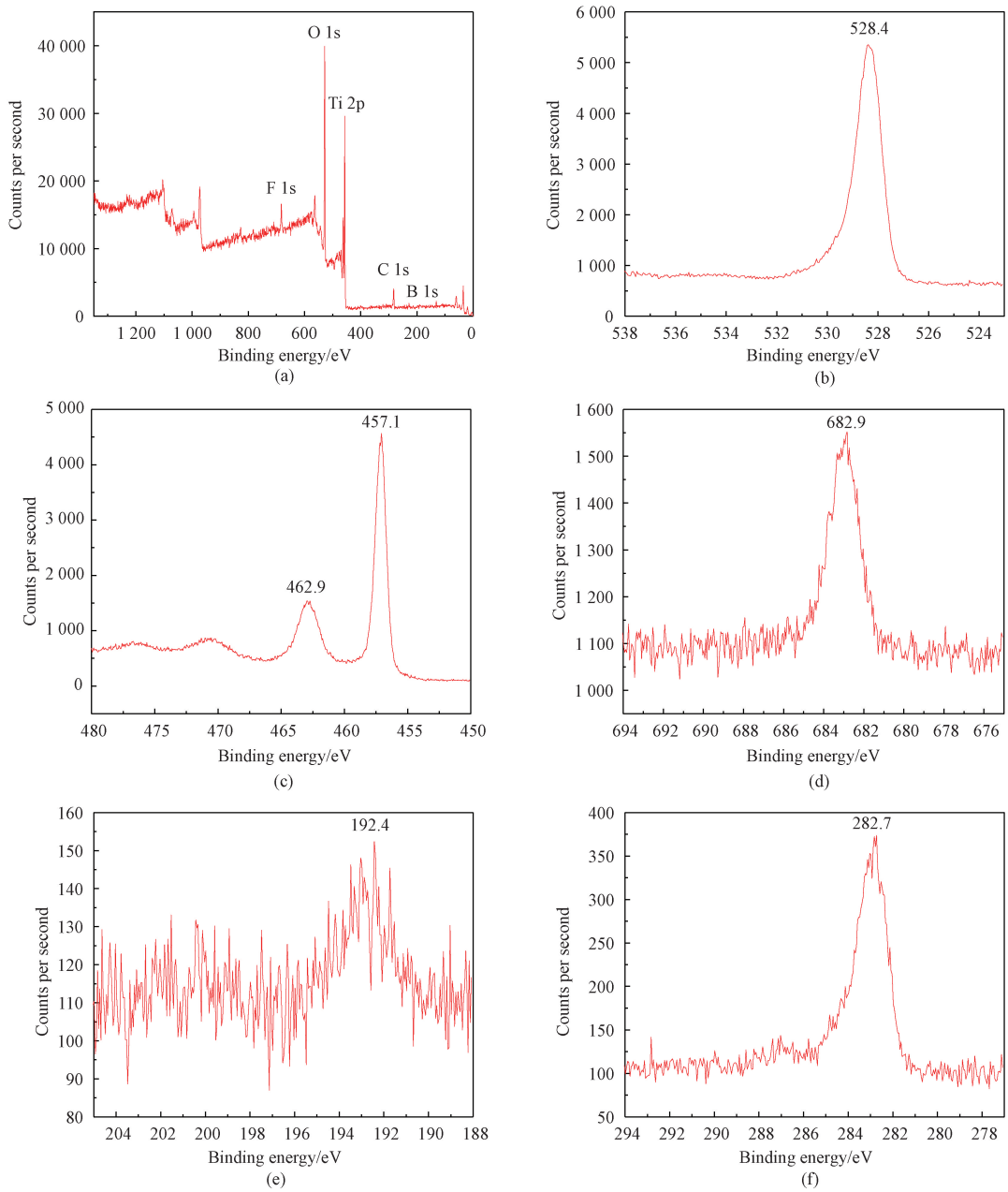

Fig. 4 XPS spectra of F-B-TiO_2-0.50: (a) survey spectrum; (b) O 1s; (c) Ti 2p; (d) F 1s; (e) B 1s; (f) C 1s

2.5 Photocatalytic hydrogen evolution performance

The photocatalytic performance of F-B-TiO_2 samples synthesized under different conditions was evaluated through the photocatalytic hydrogen evolution reaction, where methanol was employed as a sacrificial reductant, and P25 as a reference material. As shown in Fig. 5(a), the non-doped TiO_2 sample synthesized without additives exhibits the lowest photocatalytic activity. However, the photocatalytic activity of F-B-TiO_2 samples is enhanced due to F-B co-doping, reaching the highest point at a volume ratio of HBF_4 to $TiCl_3$ of 0.50. After 10 h of UV-Vis light irradiation, the hydrogen evolution of P25 is 1.86 μmol, while the hydrogen evolution of F-B-TiO_2-0.50 reaches 20.57 μmol, more than 10 times that of P25. The photocatalytic activity of F-B-TiO_2 samples synthesized at other volume ratios is significantly lower than that of F-B-TiO_2-0.50. These results are coincident with the UV-Vis absorption properties shown in Fig. 3. The photocatalytic activity of F-B-TiO_2 does not linearly increase with the added amount of HBF_4, which needs further and deeper exploration. In general, the long-term stability and reusability of photocatalysts is a crucial value for their practical applications. Therefore, corresponding experiments were performed. The cyclic test results are shown in Fig. 5(b). F-B-TiO_2-0.50 possesses excellent photostability, and there is no obvious decrease in the hydrogen evolution after three cycles.

Oxygen vacancies and defect structures also play an important role in enhancing the photocatalytic hydrogen evolution performance of F-B-TiO_2 nanosheets. These vacancies introduce mid-gap states that narrow the bandgap, extending absorption into the visible region, as confirmed by UV-Vis-NIR spectra. The mid-gap states act as shallow electron traps, facilitating charge separation and suppressing recombination, which is further supported by the presence of Ti^{3+} species in the XPS analysis. Additionally, oxygen vacancies serve as active sites for proton adsorption and reduction, lowering the activation energy for hydrogen evolution. The significant enhancement in hydrogen evolution, over 10 times that of P25, suggests their crucial role in boosting the photocatalytic activity. The correlation between the vacancy concentration and hydrogen evolution, peaking at a volume ratio of HBF_4 to $TiCl_3$ of 0.50, highlights the need for optimal defect engineering. Furthermore, SEM and TEM analyses reveal porous structures on the anatase (001) facets, providing additional charge trapping sites and enhancing surface reaction kinetics. The synergistic effects of oxygen vacancies, defect structures and F-B co-doping collectively improve charge transfer and hydrogen evolution, demonstrating the importance of defect engineering in optimizing TiO_2-based photocatalysts.

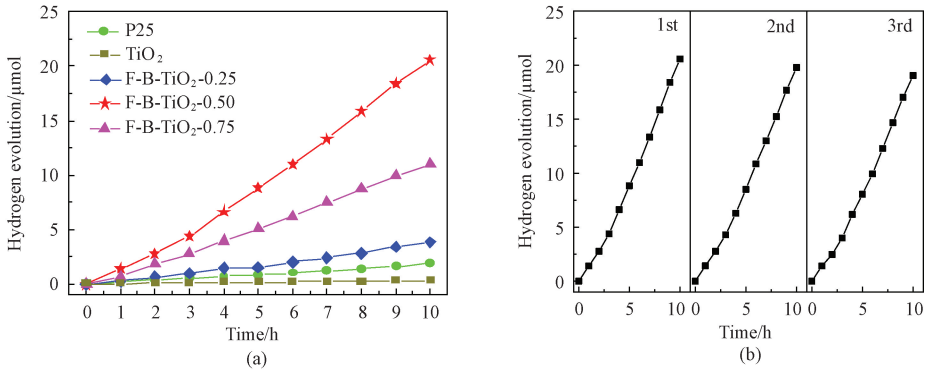

Fig. 5 Photocatalytic hydrogen evolution by different photocatalysts: (a) comparison of P25 and F-B-TiO_2 obtained at different volume ratios of HBF_4 to $TiCl_3$; (b) three repeated cycles of F-B-TiO_2-0.50

3 Conclusions

Using $TiCl_3$ and HBF_4 as precursors, F-B co-doped TiO_2 (F-B-TiO_2) nanosheets were successfully synthesized through a simple one-pot solvothermal method. The addition of HBF_4 significantly suppressed the growth of the less active anatase (101) facets and greatly promoted the exposure of the more active anatase (001) facets, ultimately forming a flower-like structure assembled from F-B-TiO_2 nanosheets bounded with dominant anatase (001) facets. Additionally, F-B co-doping led to the formation of oxygen vacancies and defect structures on the TiO_2 crystal surface, inducing the surface reconstruction of anatase nanosheets. This reconstruction, coupled with the exposed highly active anatase (001) facets and the presence of defect structures, significantly enhanced the photocatalytic performance of F-B-TiO_2, with the hydrogen evolution in photocatalytic water splitting exceeding that of P25 by more than 10 times. These results indicate that F-B-TiO_2 has great potential values in photocatalysis and other related fields such as the photodegradation of organic pollutants, dye-sensitized solar cells and optoelectronic devices.

References

[1] FUJISHIMA A, HONDA K. Electrochemical photolysis of water at a semiconductor electrode [J]. *Nature*, 1972, 238(5358): 37-38.

[2] GUO Q, ZHOU C Y, MA Z B, et al. Fundamentals of TiO_2 photocatalysis: concepts, mechanisms, and challenges [J]. *Advanced Materials*, 2019, 31(50): e1901997.

[3] SCHNEIDER J, MATSUOKA M, TAKEUCHI M, et al. Understanding TiO_2 photocatalysis: mechanisms and materials [J]. *Chemical Reviews*, 2014, 114(19): 9919-9986.

[4] MA Y, WANG X L, JIA Y S, et al. Titanium dioxide-based nanomaterials for photocatalytic fuel generations [J]. *Chemical Reviews*, 2014, 114(19): 9987-10043.

[5] CHEN X B, MAO S S. Titanium dioxide nanomaterials: synthesis, properties, modifications, and applications [J]. *Chemical Reviews*, 2007, 107(7): 2891-2959.

[6] WANG S C, LIU G, WANG L Z. Crystal facet engineering of photoelectrodes for photoelectrochemical water splitting [J]. *Chemical Reviews*, 2019, 119(8): 5192-5247.

[7] VITTADINI A, SELLONI A, ROTZINGER F P, et al. Structure and energetics of water adsorbed at TiO_2 anatase (101) and (001) surfaces [J]. *Physical Review Letters*, 1998, 81(14): 2954-2957.

[8] GONG X Q, SELLONI A. Reactivity of anatase

TiO_2 nanoparticles: the role of the minority (001) surface [J]. *The Journal of Physical Chemistry B*, 2005, 109(42): 19560-19562.
[9] LIU S, YU J G, JARONIEC M. Tunable photocatalytic selectivity of hollow TiO_2 microspheres composed of anatase polyhedra with exposed {001} facets [J]. *Journal of the American Chemical Society*, 2010, 132(34): 11914-11916.
[10] SELLONI A. Anatase shows its reactive side [J]. *Nature Materials*, 2008, 7(8): 613-615.
[11] YANG H G, SUN C H, QIAO S Z, et al. Anatase TiO_2 single crystals with a large percentage of reactive facets [J]. *Nature*, 2008, 453(7195): 638-641.
[12] YANG H G, LIU G, QIAO S Z, et al. Solvothermal synthesis and photoreactivity of anatase TiO_2 nanosheets with dominant {001} facets [J]. *Journal of the American Chemical Society*, 2009, 131(11): 4078-4083.
[13] HAN X G, KUANG Q, JIN M S, et al. Synthesis of titania nanosheets with a high percentage of exposed (001) facets and related photocatalytic properties [J]. *Journal of the American Chemical Society*, 2009, 131(9): 3152-3153.
[14] CHEN J S, TAN Y L, LI C M, et al. Constructing hierarchical spheres from large ultrathin anatase TiO_2 nanosheets with nearly 100% exposed (001) facets for fast reversible lithium storage [J]. *Journal of the American Chemical Society*, 2010, 132(17): 6124-6130.
[15] QAID S M H, GHAITHAN H M, BAWAZIR H S, et al. Successful growth of TiO_2 nanocrystals with {001} facets for solar cells [J]. *Nanomaterials*, 2023, 13(5): 928.
[16] REN L, MA S S, SHI Y, et al. Insights into the pivotal role of surface defects on anatase TiO_2 nanosheets with exposed {001} facets for enhanced photocatalytic activity [J]. *Materials Research Bulletin*, 2023, 164: 112255.
[17] LIAO S Q, LIU H, LU Y F, et al. Structural diversity design, four nucleation methods growth and mechanism of 3D hollow box TiO_2 nanocrystals with a temperature-controlled high (001) crystal facets exposure ratio [J]. *ACS Omega*, 2024, 9(1): 1695-1713.
[18] FU C, LI F, WU Z F, et al. Traces of potassium induce restructuring of the anatase TiO_2 (001)-(1 × 4) surface from a reactive to an inert structure [J]. *The Journal of Physical Chemistry Letters*, 2023, 14(40): 8916-8921.
[19] KUBIAK A, GRZEG RSKA A, GABAŁA E, et al. Unraveling a novel microwave strategy to fabricate exposed {001}/{101} facets anatase nanocrystals: potential for use to the elimination of environmentally toxic metronidazole waste [J]. *Materials Research Bulletin*, 2023, 167: 112438.
[20] SUN L M, YUAN Y Y, HE X X, et al. Hollow anatase TiO_2 tetrakaidecahedral crystals with an active {001}/{110} redox interface toward high-performance photocatalytic activity [J]. *Chemical Science*, 2024, 15(2): 692-700.
[21] BASAVARAJAPPA P S, PATIL S B, GANGANAGAPPA N, et al. Recent progress in metal-doped TiO_2, non-metal doped/codoped TiO_2 and TiO_2 nanostructured hybrids for enhanced photocatalysis [J]. *International Journal of Hydrogen Energy*, 2020, 45(13): 7764-7778.
[22] NUR A S M, SULTANA M, MONDAL A, et al. A review on the development of elemental and codoped TiO_2 photocatalysts for enhanced dye degradation under UV-vis irradiation [J]. *Journal of Water Process Engineering*, 2022, 47: 102728.
[23] WANG C, AO Y H, WANG P F, et al. Preparation, characterization and photocatalytic activity of the neodymium-doped TiO_2 hollow spheres [J]. *Applied Surface Science*, 2010, 257(1): 227-231.
[24] ASAHI R, MORIKAWA T, OHWAKI T, et al. Visible-light photocatalysis in nitrogen-doped titanium oxides [J]. *Science*, 2001, 293(5528): 269-271.
[25] TEE S Y, KONG J H, KOH J J, et al. Structurally and surficially activated TiO_2 nanomaterials for photochemical reactions [J]. *Nanoscale*, 2024, 16(39): 18165-18212.
[26] FANG W J, YAN J W, WEI Z D, et al. Account of doping photocatalyst for water splitting [J]. *Chinese Journal of Catalysis*, 2024, 60: 1-24.
[27] RUAN X W, LI S J, HUANG C X, et al. Catalyzing artificial photosynthesis with TiO_2 heterostructures and hybrids: emerging trends in a classical yet contemporary photocatalyst [J]. *Advanced Materials*, 2024, 36(17): 2305285.
[28] AYAPPAN C, XING R M, ZHANG X T, et al. TiO_2-based photocatalysts for emerging gaseous pollutants removal: from photocatalysts to reactors design [J]. *Coordination Chemistry Reviews*, 2024, 515: 215960.
[29] NAKAMURA I, NEGISHI N, KUTSUNA S, et al. Role of oxygen vacancy in the plasma-treated TiO_2 photocatalyst with visible light activity for NO removal [J]. *Journal of Molecular Catalysis A: Chemical*, 2000, 161(1): 205-212.
[30] JUSTICIA I, ORDEJÓN P, CANTO G, et al. Designed self-doped titanium oxide thin films for efficient visible-light photocatalysis [J].

Advanced Materials, 2002, 14(19): 1399-1402.
[31] GONG X Q, SELLONI A, BATZILL M, et al. Steps on anatase TiO_2 (101) [J]. *Nature Materials*, 2006, 5(8): 665-670.
[32] STRUNK J, VINING W C, BELL A T. A study of oxygen vacancy formation and annihilation in submonolayer coverages of TiO_2 dispersed on MCM-48[J]. *The Journal of Physical Chemistry C*, 2010, 114(40): 16937-16945.
[33] LIU G, YANG H G, WANG X W, et al. Enhanced photoactivity of oxygen-deficient anatase TiO_2 sheets with dominant {001} facets [J]. *The Journal of Physical Chemistry C*, 2009, 113(52): 21784-21788.
[34] THOMPSON T L, YATES J T. Surface science studies of the photoactivation of TiO_2 new photochemical processes[J]. *Chemical Reviews*, 2006, 106(10): 4428-4453.
[35] FAN C Y, CHEN C, WANG J, et al. Black hydroxylated titanium dioxide prepared via ultrasonication with enhanced photocatalytic activity [J]. *Scientific Reports*, 2015, 5: 11712.
[36] SOURI D, TAHAN Z E. A new method for the determination of optical band gap and the nature of optical transitions in semiconductors [J]. *Applied Physics B*, 2015, 119 (2): 273-279.
[37] REYES-GARCIA E A, SUN Y P, RAFTERY D. Solid-state characterization of the nuclear and electronic environments in a boron-fluoride co-doped TiO_2 visible-light photocatalyst [J]. *The Journal of Physical Chemistry C*, 2007, 111 (45): 17146-17154.
[38] ZHAO W, MA W H, CHEN C C, et al. Efficient degradation of toxic organic pollutants with $Ni_2O_3/TiO_{2-x}B_x$ under visible irradiation [J]. *Journal of the American Chemical Society*, 2004, 126(15): 4782-4783.
[39] CZOSKA A M, LIVRAGHI S, CHIESA M, et al. The nature of defects in fluorine-doped TiO_2[J]. *The Journal of Physical Chemistry C*, 2008, 112(24): 8951-8956.
[40] WANG B, LEUNG M K H, LU X Y, et al. Synthesis and photocatalytic activity of boron and fluorine codoped TiO_2 nanosheets with reactive facets [J]. *Applied Energy*, 2013, 112: 1190-1197.
[41] LI J Y, LU N, QUAN X, et al. Facile method for fabricating boron-doped TiO_2 nanotube array with enhanced photoelectrocatalytic properties [J]. *Industrial & Engineering Chemistry Research*, 2008, 47(11): 3804-3808.

暴露高活性 (001) 晶面的 F-B 共掺杂锐钛矿 TiO_2 纳米片及其光催化产氢性能

张梦瑶, 韦 莉, 刘 蕾*
东华大学 先进低维材料中心, 上海 201620

摘 要: 通过一步溶剂热合成法制备了暴露 (001) 晶面的 F-B 共掺杂锐钛矿 TiO_2 纳米片, 并研究了其光催化产氢性能。试验结果表明, 该方法能够有效促进高活性锐钛矿 (001) 晶面的生长, 增强 TiO_2 对可见光和红外光的吸收, 并进一步诱导形成氧空位。在最优化条件下, 该材料受紫外-可见光照射 10 小时后的产氢量达到 20.57 μmol, 比商品 TiO_2 纳米颗粒 Degussa P25 高出 10 倍以上。研究结果表明 F-B 共掺杂锐钛矿 TiO_2 纳米片在光催化领域具有很好的应用潜力。

关键词: F-B 共掺杂; TiO_2; 光催化; 活性晶面; 氧空穴